Induced-fit recognition of DNA by organometallic complexes with dynamic stereogenic centers

Induced-fit recognition of DNA by organometallic complexes with dynamic stereogenic centers

Haimei Chen[†], John A. Parkinson[‡], Olga Nováková[§], Juraj Bella[†], Fuyi Wang[†], Alice Dawson[†], Robert Gould[†], Simon Parsons[†], Viktor Brabec[§¶], and Peter J. Sadler[†¶]

[†]School of Chemistry, University of Edinburgh, West Mains Road, Edinburgh EH9 3JJ, United Kingdom; [‡]Department of Pure and Applied Chemistry, University of Strathclyde, Glasgow G1 1XQ, United Kingdom; and [§]Institute of Biophysics, Academy of Sciences of the Czech Republic, Kralovopolska 135, CZ-61265, Brno, Czech Republic

Edited by Jack Halpern, University of Chicago, Chicago, IL, and approved October 7, 2003 (received for review July 1, 2003)

Organometallic chemistry offers novel concepts in structural diversity and molecular recognition that can be used in drug design. Here, we consider DNA recognition by η^6-arene Ru(II) anticancer complexes by an induced-fit mechanism. The stereochemistry of the dinuclear complex $[((\eta^6\text{-biphenyl})\text{RuCl(en)})_2\text{-}(CH_2)_6]^{2+}$ (3, en = ethylenediamine) was elucidated by studies of the half unit $[(\eta^6\text{-biphenyl})\text{RuCl(Et-en)}]^+$ (2, where Et-en is $Et(H)NCH_2CH_2NH_2$). The structures of the separated $R^*_{Ru}R^*_N$ and $S^*_{Ru}R^*_N$ diastereomers of 2 were determined by x-ray crystallography; their slow interconversion in water ($t_{1/2} \approx 2$ h, 298 K, pH 6.2) was observed by NMR spectroscopy. For 2 and 3 the $R^*_{Ru}R^*_N$ configurations are more stable than $S^*_{Ru}R^*_N$ (73:27). X-ray and NMR studies showed that reactions of 2 and 3 with 9-ethylguanine gave rise selectively to $S^*_{Ru}R^*_N$ diastereomers. Dynamic chiral recognition of guanine can lead to high diastereoselectivity of DNA binding. The dinuclear complex 3 induced a large unwinding (31°) of plasmid DNA, twice that of mononuclear 2 (14°), and effectively inhibited DNA-directed RNA synthesis *in vitro*. This dinuclear complex gave rise to interstrand cross-links on a 213-bp plasmid fragment with efficiency similar to bifunctional cisplatin, and to 1,3-GG interstrand and 1,2-GG and 1,3-GTG intrastrand cross-links on site-specifically ruthenated 20-mers. Complex 3 blocked intercalation of ethidium considerably more than mononuclear 2. The concept of induced-fit recognition of DNA by organometallic complexes containing dynamic stereogenic centers via dynamic epimerization, intercalation, and cross-linking may be useful in the design of anticancer drugs.

Organometallic chemistry can provide novel concepts in structural diversity and molecular recognition that can be applied to the design of pharmaceutics (1). For example, Jaouen *et al.* (2) have designed antiestrogenic cyclopentadienyl complexes that recognize the estrogen receptor and have potential for treatment of breast cancer, and other workers have also carried out pioneering studies on the recognition of nucleobases, amino acids, and peptides by organometallic centers (1, 3–5). However, as far as we are aware, there are few investigations of specific interactions of organometallic arene complexes with natural DNA (6).

The biological chemistry of Ru(η^6-arene) complexes is relatively unexplored, although there are many reports of their use as chiral catalysts (7–9) or as synthetic reagents for peptide synthesis (3). We have discovered the anticancer potential of the ethylenediamine (en) complexes $[(\eta^6\text{-arene})\text{RuCl(en)}]^+$, which exhibit *in vitro* and *in vivo* activity, for example in a cisplatin-resistant A2780 xenograft model of human ovarian cancer (10, 11). The cytotoxicity appears to increase with increasing size of the η^6-arene. A potential target is DNA. Complexes of the type of $[(\eta^6\text{-arene})\text{RuCl(en)}]^+$ exhibit remarkably high selectivity for G compared with the other nucleobases in DNA. This is strongly related to the en NH_2 group that is attractive toward exocyclic carbonyl oxygens but repulsive toward exocyclic amino groups of nucleobases (12). In addition, hydrophobic interactions between the arene ring and nucleobase (including arene-purine π-π stacking) have a significant influence on both the kinetics and thermodynamics of DNA binding (12, 13). DNA binding modes involving simultaneous intercalation and coordination can be proposed for this type of $[(\eta^6\text{-arene})\text{RuCl(en)}]^+$ complex (14).

Here, we elaborate a multifunctional mode of DNA binding for organometallic complexes based on the linking of two $\{(\eta^6\text{-arene})\text{RuCl(diamine)}\}$ units, with a flexible chain. This introduces stereogenic centers at Ru and N, giving potential for dynamic chiral DNA recognition since epimerization at these centers is expected to be facile (15–19). Such a recognition mechanism contrasts with "static" concepts, such as "shape-match" for selective DNA recognition by octahedral metallointercalators (20).

Experimental Procedures

Synthesis. The tetraamine ligand *N*,*N*′-bis(2-aminoethyl)-1,6-diaminohexane was synthesized stepwise as the tetrahydrochloride salt (Scheme 1), which is published as supporting information on the PNAS web site. This was reacted with $[(\eta^6\text{-Bip})\text{RuCl}_2]_2$ to form the dinuclear complex $[((\eta^6\text{-Bip})\text{RuCl(en)})_2\text{-}(CH_2)_6][PF_6]_2$ [BisRu(Bip), **3**], where Bip is biphenyl. The mononuclear complex $[(\eta^6\text{-Bip})\text{RuCl(Et-en)}][PF_6]$ (**2**) was prepared by reaction of *N*-ethyl-en (Et-en) with $[(\eta^6\text{-Bip})\text{RuCl}_2]_2$. Slow diffusion of ether into a methanol solution of **2** produced crystals suitable for x-ray diffraction. Crystalline **2** consisted of a mixture of orange lumps of diastereomer **2A**($R^*_{Ru}R^*_N$) and yellow flakes of diastereomer **2B** ($S^*_{Ru}R^*_N$), which were separated by hand. The 9-ethylguanine (9EtG) adducts $[(\eta^6\text{-Bip})\text{Ru}(N7\text{-9EtG})\text{(Et-en)}]^{2+}$ (**4**) and $[((\eta^6\text{-Bip})\text{Ru}(N7\text{-9EtG})\text{(en)})_2\text{-}(CH_2)_6]^{4+}$ (**5**) were prepared by reactions of 9EtG with **2** or $[((\eta^6\text{-Bip})\text{Ru}(H_2O)\text{(en)})_2\text{-}(CH_2)_6]^{4+}$ (**3ww**) in water (G/Ru = 1.2:1). Recrystallization of **4** (PF_6^- salt) from methanol gave yellow crystals suitable for x-ray diffraction. Full details of synthesis and characterization are in the *Supporting Text*, which is published as supporting information on the PNAS web site.

Kinetic Studies. Reactions of chloro or aqua complexes **1-3** (2.55 mM Ru, except 0.5 mM for **3**) with 9EtG in a 1:1 Ru/9EtG molar ratio were carried out in 10% D_2O/90% H_2O in NMR tubes. Aqua complexes were prepared by treatment of chloro com-

This paper was submitted directly (Track II) to the PNAS office.

Abbreviations: Bip, biphenyl; dien, diethylenetriamine; CT, calf thymus; en, ethylenediamine; 9EtG, 9-ethylguanine.

Data deposition: The x-ray crystal structures of complexes **2A**, **2B**, and **4** have been deposited in the Cambridge Structural Database, Cambridge Crystallographic Data Centre, Cambridge CB2 1EZ, United Kingdom, (CSD reference nos. 223919, 223918, and 223917, respectively).

¶To whom correspondence should be addressed. E-mail: brabec@ibp.cz or p.j.sadler@ed.ac.uk.

plexes with a stoichiometric amount of $AgNO_3$. Interconversion of diastereomers **2A** and **2B** (0.5 mM Ru) was studied in D_2O in NMR tubes. When necessary, 180 mM NaCl was used to suppress hydrolysis. Interconversion rate constants (k_1, **2A** $\rightarrow$ **2B**; k_{-1}, **2B** $\rightarrow$ **2A**) were obtained by fitting rate equations for first-order reversible reactions by using the program SCIENTIST (version 2.0, MicroMath, St. Louis).

DNA Modification. Calf thymus (CT) DNA and plasmid DNAs were incubated with metal complexes in 10 mM $NaClO_4$ at 310 K for 48 h in the dark, unless stated otherwise. The molar ratios of bound metal complex to nucleotide phosphate (r_b) were determined by flameless atomic absorption spectrophotometry. CD spectra of DNA modified by **3** were recorded at 298 K on a Jasco (Tokyo) J-720 spectropolarimeter, after samples had been incubated for 24 h at 310 K and then dialyzed for 2 days at 277 K in 10 mM $NaClO_4$.

DNA Transcription by RNA Polymerase *in Vitro*. Transcription of the (*Nde*I/*Hpa*I) restriction fragment of pSP73KB DNA with SP6 or T7 RNA polymerase and electrophoretic analysis of transcripts were performed according to the protocols recommended by Promega as described (21). Before aliquots containing the transcripts were loaded on the polyacrylamide gel, the radioactivity associated with these samples was adjusted so that equal amounts of radioactivity were loaded into each well. For comparative purposes, the intensity at each site was determined by calculating the peak area and the background was subtracted. The average relative intensities of each band from three independent experiments were compared.

Unwinding of Negatively Supercoiled DNA. Unwinding of closed circular supercoiled pSP73KB plasmid DNA was studied by an agarose gel mobility-shift assay (22). The mean unwinding angle $\Phi = 18\ \sigma/r_b(c)$, where σ is the superhelical density, and $r_b(c)$ the value of r_b at which the supercoiled and nicked forms comigrate. Under the present experimental conditions, σ was calculated to be -0.063 based on cisplatin for which $\Phi = 13°$. Experimental details are given in *Supporting Text*.

X-Ray Crystallography. Diffraction data for all compounds were collected with Mo-Kα radiation, for **2A**, at 220 K on a Stoe (Darmstadt, Germany) Stadi-4 diffractometer, for **2B** and **4** at 150 K on a Bruker-AXS (Madison, WI) SMART APEX CCD diffractometer; both were equipped with Oxford Cryosystems (Long Hanborough, U.K.) low-temperature devices. Absorption corrections were carried out by using ψ-scans or the multiscan procedure SADABS (23). All structures were solved by direct methods and refined against F^2 by using all data [SHELXTL (24) for **2A** and **2B**, CRYSTALS (25) for **4**]. H atoms were placed in calculated positions, and non-H atoms were modeled with anisotropic displacement parameters. WEBLAB VIEWERPRO 4.0 was used for the graphics in Fig. 2.

NMR Spectroscopy. NMR data were acquired on Bruker DMX 500 (^{1}H = 500 MHz) and Avance 600 (^{1}H = 600 MHz) spectrometers. Standard pulse sequences were used for 2D heteronuclear single quantum coherence (HSQC), total correlation spectroscopy, COSY, double quantum filtered COSY, NOESY (mixing time up to 1,000 ms), and rotating-frame Overhauser effect spectroscopy (mixing time 150 ms). The water resonance was suppressed via the double pulsed-field-gradient spin-echo method (26). 2D [^{1}H,^{15}N] HSQC NMR spectra were acquired for complexes **2-5** with ^{15}N in natural abundance. Data processing was carried out by using XWIN-NMR (version 3.0, Bruker Biospin, Karlsruhe, Germany). ^{1}H NMR chemical shifts were internally referenced to $(CD_2H)_2SO$ (2.50 ppm), $(CD_2H)_2CO$ (2.06 ppm), sodium 3-(trimethylsilyl)-2,2,3,3-d$_4$-propionate (0 ppm), or dioxane (3.76 ppm), and ^{15}N to 1 M $^{15}NH_4Cl$ in 1.5 M HCl (external) at 0 ppm.

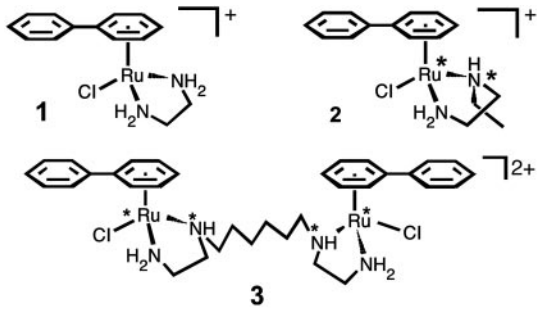

Fig. 1. Structures of mono- and bis-Ru(Bip) chloride complexes. * indicate stereogenic centers.

Molecular Modeling. Modeling was carried out by using SYBYL (version 6.3, Tripos Associates, St. Louis) by docking a model of {((η^6-Bip)Ru(*N7*-G)(en))$_2$-$(CH_2)_6$}, based on the x-ray structure of **4**, onto B-form duplex DNA 5′-AAT**G**TCTAA-3′/3′-TTACA**G**ATT-5′.

Supporting Information. Full details for experimental procedures (materials, synthesis, acidity constants, DNA experiments, and kinetics), Tables 1–4 (crystallographic data, rate constants, half-lives, equilibrium constants), and Figs. 6–21 (^{1}H NMR, 2D COSY, heteronuclear single quantum coherence, NOESY, and rotating-frame Overhauser effect spectroscopy spectra for **2-5**; kinetics of 9EtG and CT DNA binding, cross-linking, ethidium fluorescence, modeling) are published as supporting information on the PNAS web site.

Results and Discussion

Stereogenic Preferences and Epimerization Rates. We synthesized the dinuclear complex [((η^6-Bip)RuCl(en))$_2$-$(CH_2)_6]^{2+}$ [BisRu(Bip), **3**] by linking two {(η^6-Bip)RuCl(en)} units with a hexamethylene chain, which is long and flexible enough to allow each Ru unit to behave independently (Fig. 1). The strategy of linking two or three Pt centers has already been used successfully in drug design (27). Complex **3** contains four stereogenic centers (Ru, N, N, Ru), giving rise to 10 possible configurations (Fig. 13). Studies of the mononuclear analogue [(η^6-Bip)RuCl(Et-en)]$^+$ (**2**), which contains similar stereogenic Ru and N centers, allowed subsequent elucidation of the structure and dynamics of **3**.

Synthesis of **2** gave rise to two diastereomers **2A**($R^*_{Ru}R^*_N$) and **2B**($S^*_{Ru}R^*_N$) (28)‖ in a 73.7:26.3 mol ratio, as revealed by x-ray crystallography (Figs. 2 and 6) and NMR studies (Figs. 8–11). The 2D [^{1}H,^{15}N] heteronuclear single quantum coherence NMR spectra of **2** and **3** in DMSO-d_6 are almost identical (Fig. 8), suggesting that each Ru unit of **3** is present as either an **A**($R^*_{Ru}R^*_N$) or **B**($S^*_{Ru}R^*_N$) configuration and that each Ru unit has little influence on the other. Complex **3** can be treated as a diastereomeric mixture of **AA** (I), **AB** (II), and **BB** (III) (Figs. 3*A*, 12, and 13). The **AA**/**AB**/**BB** ratio was determined to be 67.7:24.0:8.3 by 2D total correlation spectroscopy NMR (Fig. 3*B*), consistent with that of 72.9:27.1 for **A**/**B** from 2D [^{1}H,^{15}N] NMR (Fig. 8*ii*).

The displacement of Cl by H_2O appears to have negligible

‖The formal absolute configuration at Ru was determined by using the general priority order: Bip > Cl/O/N7 > N2 > N1 for diastereomers **2A**(Cl, H_2O), **2B**(Cl, H_2O), and **4**(*N7*-9EtG) (28). No CD signals were detected for **2A**, **2B**, or **4** in DMSO or water, consistent with each diastereomer being present as an enantiomeric pair in a 1:1 ratio as in the crystals.

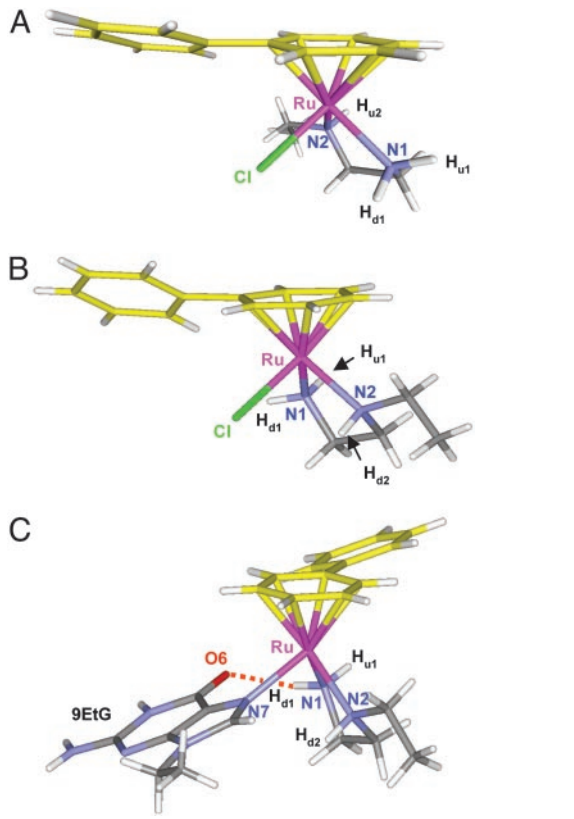

Fig. 2. Structures of $R_{Ru}R_N$ (**2A**) (*A*) and $S_{Ru}R_N$ (**2B**) (*B*) diastereomers of $[(\eta^6\text{-Bip})RuCl(Et\text{-}en)]^+$, and $S_{Ru}R_N$ (**4**) diastereomer of $[(\eta^6\text{-Bip})Ru(N7\text{-}9EtG)(Et\text{-}en)]^{2+}$ (*C*) [H-bonds O6···H-N1: O6···N1 2.840 (7) Å, ∠N1-H···O6 160.72°]. Their respective enantiomers **2A′**($S_{Ru}S_N$), **2B′**($R_{Ru}S_N$), and **4′**($R_{Ru}S_N$) are present in the same unit cell. In text, labels **A**($R^*_{Ru}R^*_N$) and **B**($S^*_{Ru}R^*_N$) refer to the enantiomeric pairs **A**($R_{Ru}R_N/S_{Ru}S_N$) and **B**($S_{Ru}R_N/R_{Ru}S_N$). Crystallographic data are in Tables 1 and 2. Note that H on N2 points toward the coordinated arene in **A**($R^*_{Ru}R^*_N$) but away in **B**($S^*_{Ru}R^*_N$).

influence on the configurational abundance of **A** ($R^*_{Ru}R^*_N$) and **B** ($S^*_{Ru}R^*_N$) for the aqua complexes **2w** and **3ww** (for structures, see Fig. 7), as revealed by NMR, the ratio of 77:23 was found for **2Aw** ($R^*_{Ru}R^*_N$)/**2Bw**($S^*_{Ru}R^*_N$). The ^{1}H NMR spectrum for the linker of **3ww** showed a similarly complicated pattern as for **3** (Cl,Cl) and indicated that the aqua Ru units adopt both **A** ($R^*_{Ru}R^*_N$) and **B** ($S^*_{Ru}R^*_N$) configurations, with type **A** predominating as for **3** (Cl,Cl). Under the present experimental conditions, **2Aw** and **2Bw** are largely protonated since the pK_a (H_2O) values are 7.57(± 0.01) and 7.35(± 0.01), respectively (Fig. 17).

The dynamic interconversion of diastereomers **2A** and **2B** was studied by ^{1}H NMR spectroscopy at 298 K. Separated **2A** (or **2B**) was observed to convert slowly into **2B** (or **2A**) on dissolution in D_2O (containing 180 mM NaCl to suppress hydrolysis) (Figs. 7 and 9), with the equilibrium ratio of **2B**/**2A** = 28:72 (Table 3). The rate constant was determined to be k_{-1} 4.3×10^{-3} min^{-1} for **2B**(Cl) → **2A**(Cl), 2.5 times faster than the reverse reaction (k_1 1.7×10^{-3} min^{-1}) at pH 6.2, half-life 117 min (Table 3). The inversion rate at N for *R*/*S*(N)-[$PtCl_2$(*R*-2-[2-methyl-2-aminopropyl)amino]-1-butanol)] is reported to be of a similar order of magnitude (18). With no added NaCl, a stepwise conversion from **2A**(Cl) to **2A**(H_2O), to **2B**(H_2O), then to **2B**(Cl) was observed with a half-life of 150 min (Figs. 7*i* and 9*iv*). The equilibrium ratio was 18.5 **2A**(Cl):52.2 **2A**(H_2O):9.5 **2B**(Cl):19.8 **2B**(H_2O). The interconversion rate was slightly faster at pH 2.0 ($t_{1/2}$ 98 min), but much faster at pH 9.2 ($t_{1/2}$ 60 min, Table 3). No interconversion was observed in DMSO solution (Fig. 9*i*).

Each Ru unit of **3**(Cl or H_2O) can be envisioned to undergo a similar interconversion process in aqueous solution, giving rise to the same observed equilibrium ratio of 72 **A**:28 **B** as for **2**. Our studies suggest that for both **2** and **3** (Cl or H_2O) the **A**($R^*_{Ru}R^*_N$) configurations are thermodynamically preferred, and that each Ru unit is in dynamic equilibrium between configurations **A**($R^*_{Ru}R^*_N$) and **B**($S^*_{Ru}R^*_N$).

Diastereoselectivity in Guanine N7 Recognition. Reaction of 9EtG with the diastereomeric mixture of **3** (**A**/**B** = 72.9:27.1) or **2** (**A**/**B** = 73.7:26.3) gave rise to the final products $[((\eta^6\text{-Bip})Ru(N7\text{-}9EtG)(en))_2\text{-}(CH_2)_6]^{4+}$ (**5**) and $[(\eta^6\text{-Bip})Ru(N7\text{-}9EtG)(Et\text{-}en)]^{2+}$ (**4**), respectively, with ≈90% formation (Fig. 7). N7 coordination for **4**, **5**, and **3gw** [intermediate (9EtG-*N7*)Ru~Ru(H_2O)] was confirmed by pH titrations, giving associated pK_a values: pK_a(G N1H) 8.03 (**4**), 7.83 (**3gw**), 7.86 (**5**), compared with 9.66(G N1H) and 2.4(G N7) for free 9EtG (Figs. 7 and 14).

Analysis of the configurations of **5** was aided by the structural analysis of **4**. X-ray crystallography (Figs. 2*C* and 6*iv*) and NMR studies (Figs. 8 and 15) showed that **4** contains a single (95%) diastereomeric pair **B**($S^*_{Ru}R^*_N$), with the N2 H_{d2} proton pointing down toward the G base. Complex **5** showed one set of en NH crosspeaks in the 2D [^{1}H,^{15}N] heteronuclear sequential quantum correlation NMR spectrum (acetone-d_6), almost identical to that for **4** (Fig. 8), indicating that each Ru unit of **5** has the same configuration **B**($S^*_{Ru}R^*_N$) as for **4.** This was confirmed by other 2D NMR data (Figs. 3*C* and 16).

The **B**($S^*_{Ru}R^*_N$) configurations are therefore highly favored (95%) for the 9EtG adducts **4** and **5** (Figs. 7 and 8), whereas the **A**($R^*_{Ru}R^*_N$) configurations are strongly destabilized by steric interactions between G and the en alkyl substituent. This finding is in contrast to their parent chloro complexes **2** or **3** and their aqua adducts, for which the **A**($R^*_{Ru}R^*_N$) configuration is thermodynamically preferred (72%) and in which the en alkyl substituent points down toward Cl or H_2O. Displacement of Cl or H_2O by 9EtG forces the alkyl substituent to tilt up and to give the **B** configuration, which can be stabilized by stereospecific H bonding between en NH and G O6 (Fig. 2). Facile epimerization at Ru or N centers appears to allow dynamic switching between configurations, leading to high diastereoselectivity in the formation of G adducts.[††] In a reported study (5), reaction of the diastereomeric mixture of $[(\eta^6\text{-}C_6H_6)RuCl(L\text{-}ala)]$ with 9EtG did not change the abundance of $R_{Ru}S_C$ and $S_{Ru}S_C$ (65:35). In this case, the α–C center has a fixed configuration S_C and no epimerization potential; its methyl substituent is distant from the G base and has little influence on the reaction.

Structural and dynamic studies of interactions of 9EtG with **3** and **2** provided insights into the recognition of natural DNA by **3**. Substitution of an en NH proton in **1** by the alkyl group to give **2** or **3** (Fig. 1) had little effect on the kinetics of reaction of the chloro complexes with CT DNA (**1**, $t_{1/2}$ 10 min; **3**, $t_{1/2}$ 15 min), or on reactions of the aqua (**1w**, **2w**, **3ww**: $t_{1/2}$ ≈35 min) or chloro (**1**, **2**: $t_{1/2}$ ≈85 min) complexes with 9EtG (Table 4). All of these reactions were >80% complete, indicating that the alkyl substituent does not significantly hinder G binding when epimerization is facile.

Dinuclear BisRu(Bip) Distorts DNA. The dinuclear complex **3** binds rapidly to CT DNA (Fig. 18). The binding was stable with little loss of bound Ru after extensive dialysis in 0.01 M $NaClO_4$ or

[††]NMR data for the 5′ GMP adducts $[(\eta^6\text{-Bip})Ru(N7\text{-}5'GMP)(Et\text{-}en)]^{2+}$ (H8: 8.73 and 8.82 ppm) and $[((\eta^6\text{-Bip})Ru(N7\text{-}5'GMP)(en))_2\text{-}(CH_2)_6]^{4+}$ (H8: 8.72 and 8.83 ppm) are consistent with this interpretation. ^{1}H NMR peaks for the $S_{Ru}R_N$-(β-D) and $R_{Ru}S_N$-(β-D) diastereomers were present in a 1:1 mol ratio (10% D_2O, pH 7.2), suggesting that there may be no enantioselectivity between $S_{Ru}R_N$ and $R_{Ru}S_N$ for DNA binding.

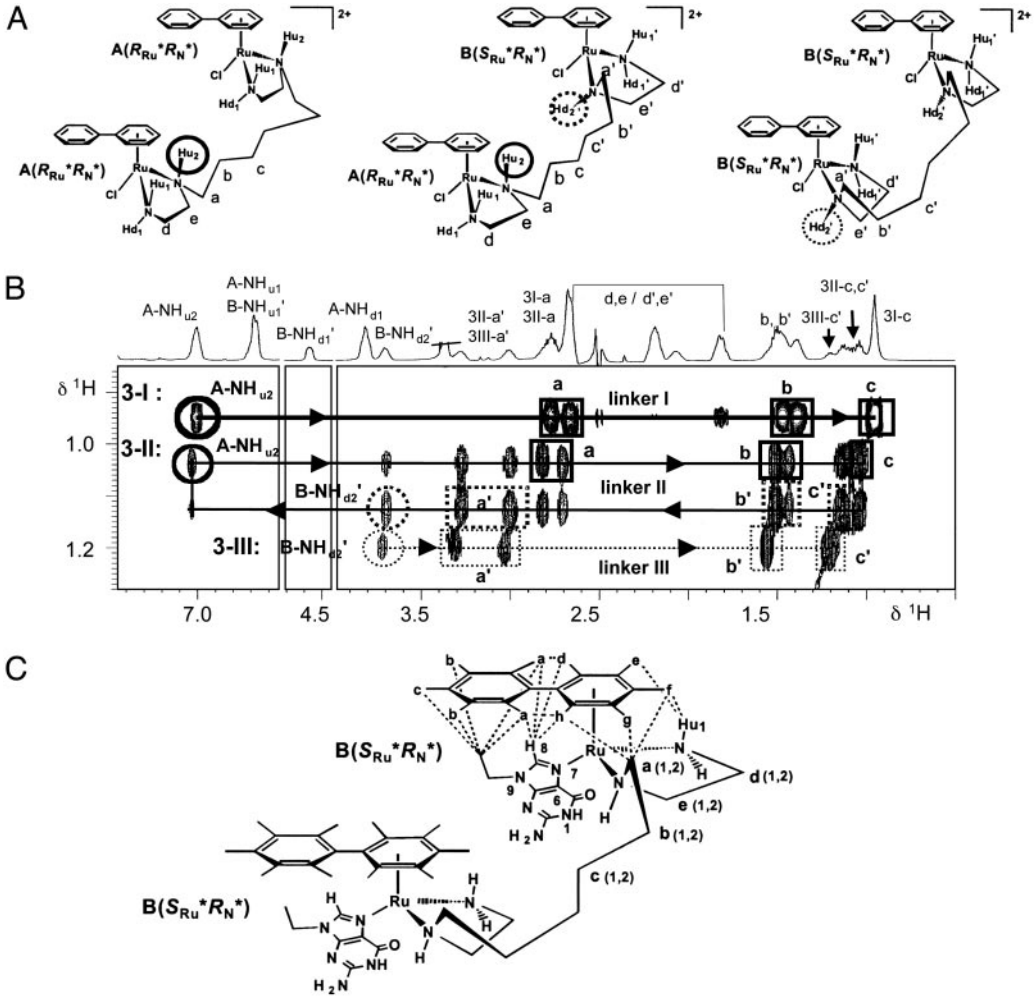

Fig. 3. Configurations of dinuclear complexes **3** and **5**. (*A*) Diastereomers **AA** (**3-I**, 68%), **AB**, (**3-II**, 24%) and **BB** (**3-III**, 8%) for **3**, with species distribution (%) based on 2D total correlation spectroscopy (TOCSY) cross-peak intensities. For full structures, see Fig. 13. (*B*) 2D TOCSY NMR spectrum of en NH and linker CH_2 region of **3** in DMSO-d_6, showing three spin-systems, with cross-peak connectivities of NH_{u2}→a→b→c for **3-I** (thick solid line), NH_{u2}→a→b→c→c′→b′→a′→NH_{d2}′ for **3-II** (thin solid line), and NH_{d2}′→a′→b′→c′ for **3-III** (dotted line). (*C*) Structure of 9EtG adduct **5** with rotating-frame Overhauser effects indicated by dotted lines. A single set of signals for **5** was detected by 2D NMR (Figs. 8*iv* and 16), suggesting the presence of **B**($S^*_{Ru}R^*_N$) configuration for each Ru unit and *syn* conformation for the pendant phenyl ring with respect to 9EtG. Adduct **5** is mainly present as configuration **BB** (95%). Labels a-e and a′-e′ represent a pair of (nonequivalent) protons on the same C.

1.0 M NaCl. An assay of DNA-directed RNA synthesis revealed that each Ru unit of **3** coordinates preferentially to G bases of DNA (Fig. 4). Complex **3** shows termination sequences somewhat different from cisplatin, although the intensity of the bands corresponding to major stop sites was similar (Fig. 4*A*). Furthermore, adducts of complex **3** inhibit RNA synthesis more effectively than those of mononuclear complexes **1** (14), **2** (Fig. 4*A*), and **2A** (data not shown). The pattern of stop sites for transplatin is different, and no termination is observed for monofunctional $[Pt(dien)Cl]^+$ (dienPt, Fig. 4*A*), where dien is diethylenetriamine. The higher sequence preference of **3** for G can be attributed to interactions with en NH, being attractive toward exocyclic carbonyl oxygens but repulsive toward exocyclic amino groups of nucleobases (12). We can assume that binding of **3** to double-helical DNA involves dynamic chiral recognition in a similar manner to the reaction of **3** with 9EtG (Figs. 7*iii* and 3*C*), with preferential formation of the **B**($S^*_{Ru}R^*_N$) configuration. This allows most of **3** (84%) to coordinate to DNA.

Conformational distortions of DNA induced by **3** are evident from CD spectra (Fig. 5*A*). Binding of **3** to CT DNA induced a positive CD band centered ≈370−380 nm with increasing intensity as a function of r_b. This band may arise from coupling between the transition dipole moment of nucleobases and the bound metal complex, suggesting intercalation of the extended phenyl ring into DNA, or groove binding (29). This spectral change is similar to that observed for mononuclear **1** (14). Such induced CD bands are not observed for reaction of CT DNA with the analogs $[(\eta^6\text{-}p\text{-cymene})RuCl(en)]^+$ and $[(\eta^6\text{-benzene})RuCl(en)]^+$ where the *p*-cymene or benzene ring cannot insert into DNA base pairs.

The CD results correlate with those of plasmid DNA unwinding. A large unwinding angle of 31° per dinuclear complex was induced by binding of **3** to pSP73KB DNA (Fig. 5*B*), twice that for the mononuclear complexes **1** (14°) (14) and **2** (14°, Fig. 5*C*) and **2A** (data not shown). Previous studies (14) have shown that **1** induces an unwinding angle twice that of $[(\eta^6\text{-}p\text{-cymene})RuCl(en)]^+$ (7°) because of the contribution from the Bip ring, possibly by intercalation. Compared with the DNA unwinding induced by the linkage isomers *cis*-$[Pt(NH_3)_2(N3/N8\text{-ethidium})Cl]^{2+}$ [15°/19° (22)], the dinuclear complex $[\{trans\text{-}PtCl(NH_3)_2\}_2\text{-}H_2N(CH_2)_6NH_2]^{2+}$ [10° (30)], trinuclear

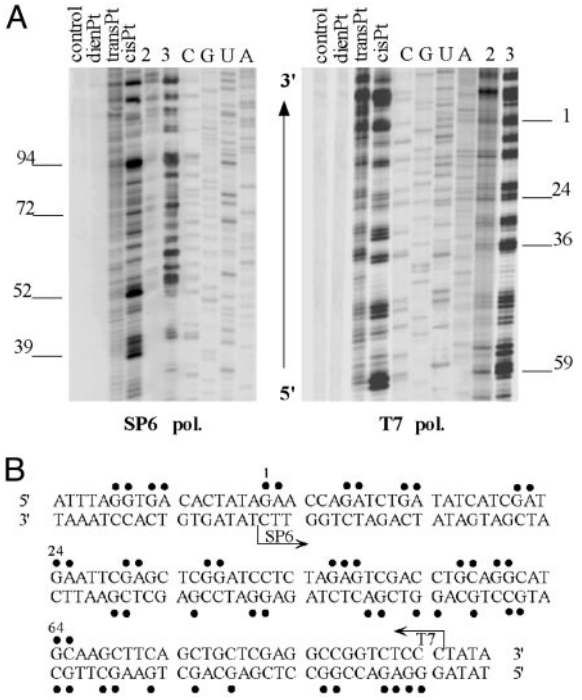

Fig. 4. Inhibition of RNA synthesis. (*A*) Autoradiograms of 6% polyacrylamide/8 M urea sequencing gels showing inhibition of RNA synthesis by SP6 (*Left*) or T7 RNA polymerases (*Right*) on the *Nde*I/*Hpa*I fragment containing adducts of Ru and Pt complexes (r_b 0.01). Lanes are: unmodified template control; templates modified by dienPt, transPt, cisPt, **2** and **3**; C, G, U and A (chain terminated marker RNAs). (*B*) Schematic diagram showing portion of sequence used to monitor inhibition of RNA synthesis by **3**. Arrows indicate start of SP6 and T7 RNA polymerase, which used the bottom or upper strand of *Nde*I/*Hpa*I fragment as templates. ● indicate major stop signals (from *A*) for **3**. Numbers correspond to nucleotide numbering in the sequence map of pSP73KB plasmid.

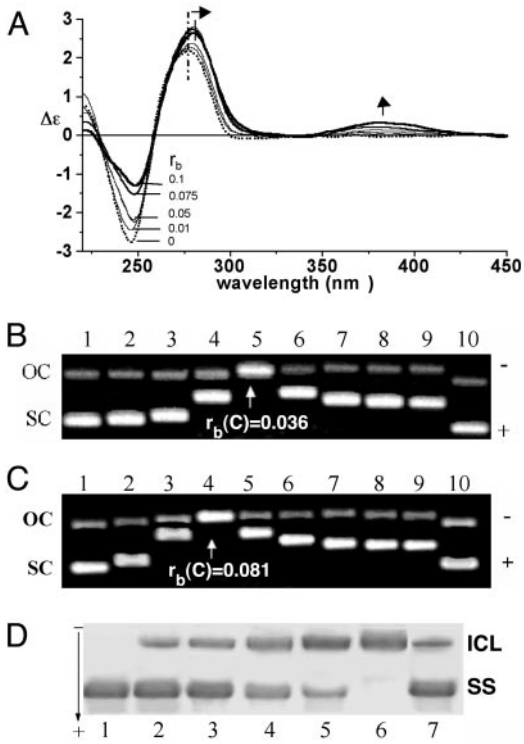

Fig. 5. (*A*) CD spectra of CT DNA modified by **3** (298 K, r_b 0–0.1, DNA 30 $\mu g \cdot ml^{-1}$). (*B*) Unwinding of supercoiled pSP73KB plasmid DNA by **3**. Plasmid DNA modified by **3** with r_b values of 0.004, 0.008, 0.017, 0.036, 0.05, 0.067, 0.076, and 0.084 corresponds to lanes 2–8. Lanes 1 and 10 show control, unmodified DNA ($r_b = 0$). The coalescence point (comigration of OC and SC) corresponds to r_b(c) of 0.036 and unwinding angle Φ of 31 ± 2°. (*Upper*) Nicked plasmid, open circular (OC); (*Lower*) closed negatively supercoiled plasmid (SC). (*C*) Unwinding of supercoiled pSP73KB plasmid DNA by **2**. Plasmid DNA modified by **2** with r_b values of 0.03, 0.06, 0.081, 0.10, 0.11, 0.13, 0.16, and 0.17 corresponds to lanes 2–8. Lanes 1 and 10 indicate control, unmodified DNA ($r_b = 0$). The coalescence point corresponds to r_b(c) of 0.081 and unwinding angle Φ of 14 ± 2°. (*D*) Formation of interstrand cross-links by dinuclear **3** and cisplatin in linear *Nde*I/*Eco*RI fragment of pSP73 plasmid (213 bp). Autoradiogram of native 1% agarose gel of 3′ end-labeled DNA fragment. Interstrand cross-linked (ICL) DNA appears as the top bands migrating more slowly than single-stranded (SS) DNA in the bottom bands. Fragment modified by **3** with r_b of 0.015, 0.03, 0.05, 0.08, and 0.10 corresponds to lanes 2–6, and by cisplatin with r_b of 0.015 corresponds to lane 7. Lane 1 indicates nonmodified fragment (control).

BBR3464 [14° (31)], and mononuclear transplatin (9°), the larger unwinding angle (31°) induced by **3** can be attributed to cross-linking of DNA and perturbation of DNA structure by the two pendant phenyl rings. Additionally, complex **3** blocked intercalation of ethidium (about two times) more effectively than mononuclear **2** (Fig. 20), and **2** is more effective than $[(\eta^6\text{-}p\text{-cymene})RuCl(en)]^+$ (14) or $[Pt(dien)Cl]^+$ (Fig. 20). These results suggest that both the linker chain and phenyl rings contribute to the interaction.

The Bip ligand possesses fluxionality through rotation around the arene-Ru bonds and propeller twisting of Bip (13). NMR studies on the 9EtG products **4** (Fig. 15) and **5** (Fig. 3*C*) show that in solution the guanine base is *syn* to the pendant phenyl ring, indicating potential hydrophobic interactions between Bip and nucleobase (13), which could stabilize intercalation into duplex DNA.

Further evidence for DNA cross-linking by **3** was obtained. The efficiency of interstrand cross-linking on a 213-bp *Nde*I/*Eco*RI fragment of pSP73 randomly modified by **3** (≈5% frequency) was similar to that for cisplatin (Fig. 5*D*), and a site-specifically ruthenated 20-mer formed a 1,3-GG (5′ to 5′) interstrand cross-link (20% frequency, Fig. 19). Studies of -TGGT- and -TGTGT- 20-mer duplexes showed that complex **3** is also able to form intrastrand 1,2-GG and 1,3-GTG cross-links. A model for possible 1,3 interstrand cross-linking by **3** on B-form duplex DNA (5′-AAT**G**TCTAA-3′/3′-TTACA**G**ATT-5′) is shown in Fig. 21. Each Ru unit adopts the $\mathbf{B}(S^*_{Ru}R^*_N)$ configuration, and the two Ru atoms are coordinated to N7 of G4 and G13 with en NH H-bonding to G O6. The pendant phenyl ring from each Bip is partially intercalated into the DNA base pairs. Modeling therefore suggests that the multifunctional interactions with DNA proposed for **3** are compatible.

In contrast to octahedral metallointercalators such as Tris(phenanthroline)Ru(II) derivatives (20, 32), [Ru(phenanthroline)$_2$Cl$_2$] (33), and [Ru(bipyridine)$_2$Cl$_2$] (34), which are essentially inert to racemization, have rigid frameworks, and recognize DNA mainly by shape-match (20), the $\{(\eta^6\text{-arene})Ru(II)\}$ complexes studied here have dynamic stereogenic centers and fluxional η^6-arene ligands. Binding of these Ru(arene) complexes to DNA can be accompanied by configurational changes that allow recognition by an induced fit mechanism. It should be possible to enhance DNA recognition by modification of the chelate en, the linker and the arene ring system. DNA is also flexible and can optimize its fit with Ru(arene) via unwinding, base-twisting, and bending (35). Distortions of DNA structure are recognized by downstream processing, including protein binding (36), and can play an important role in anticancer activity. Such considerations may aid the design of clinically more effective antitumor drugs, and thus

expand the potential of organometallic (η^6-arene)Ru(II) complexes in medicine.

We thank European Community Cooperation in Science and Technology Action D20 and Dr. D. Jodrell and colleagues (Western General Hospital, Edinburgh) for stimulating discussions and Drs. E. Zhang and P. Wang for advice on amine synthesis. We thank the Committee of Vice-Chancellors and Principals for an Overseas Research Scholarship Award (to H.C.), the Wellcome Trust, the Grant Agency of the Czech Republic (Grants 305/02/1552 and 305/01/0418) and the Grant Agency of the Academy of Science of the Czech Republic (Grant A5004101) for support.

1. Fish, R. H. & Jaouen, G. (2003) *Organometallics* **22,** 2166–2177.
2. Jaouen, G., Vessières, A. & Butler, I. S. (1993) *Acc. Chem. Res.* **26,** 361–369.
3. Severin, K., Bergs, R. & Beck, W. (1998) *Angew. Chem. Int. Ed.* **37,** 1634–1654.
4. Kuo, L. Y., Kanatzidis, M. G., Sabat, M., Tipton, A. L. & Marks, T. J. (1991) *J. Am. Chem. Soc.* **113,** 9027–9045.
5. Sheldrick, W. S. & Heeb, S. (1990) *Inorg. Chim. Acta* **168,** 93–100.
6. Gopal, Y. N. V., Jayaraju, D. & Kondapi, A. K. (1999) *Biochemistry* **38,** 4382–4388.
7. Consiglio, G. & Morandini, F. (1987) *Chem. Rev.* **87,** 761–778.
8. Faller, J. W., Patel, B. P., Albrizzio, M. A. & Curtis, M. (1999) *Organometallics* **18,** 3096–3104.
9. Davies, D. L., Fawcett, J., Garratt, S. A. & Russell, D. R. (2001) *Organometallics* **20,** 3029–3034.
10. Aird, R. E., Cummings, J., Ritchie, A. A., Muir, M., Morris, R. E., Chen, H., Sadler, P. J. & Jodrell, D. I. (2002) *Br. J. Cancer* **86,** 1652–1657.
11. Morris, R. E., Aird, R. E., del Socorro Murdoch, P., Chen. H., Cummings, J., Hughes, N. D., Parsons, S., Parkin, A., Boyd, G., Jodrell, D. I. & Sadler, P. J. (2001) *J. Med. Chem.* **44,** 3616–3621.
12. Chen, H., Parkinson, J. A., Morris, R. E. & Sadler, P. J. (2003) *J. Am. Chem. Soc.* **125,** 173–186.
13. Chen, H., Parkinson, J. A., Parsons, S., Coxall, R. A., Gould, R. O. & Sadler, P. J. (2002) *J. Am. Chem. Soc.* **124,** 3064–3082.
14. Novakova, O., Chen, H., Vrana, O., Rodger, A., Sadler, P. J. & Brabec, V. (2003) *Biochemistry* **42,** 11544–11554.
15. Brunner, H. (2001) *Eur. J. Inorg. Chem.* 905–912.
16. Faller, J. W., Parr, J. & Lavoie, A. R. (2003) *New J. Chem.* **27,** 899–901.
17. Buckingham, D. A., Marzilli, L. G. & Sargeson, A. M. (1969) *J. Am. Chem. Soc.* **91,** 5227–5232.
18. Saito, R., Goto, M., Hirose, J. & Kidani, Y. (1992) *Bull. Chem. Soc. Jpn.* **65,** 1428–1437.
19. Williams, K. M., Scarcia, T., Natile, G. & Marzilli, L. G. (2001) *Inorg. Chem.* **40,** 445–454.
20. Erkkila, K. E., Odom, D. T. & Barton, J. K. (1999) *Chem. Rev.* **99,** 2777–2795.
21. Brabec, V. & Leng, M. (1993) *Proc. Natl. Acad. Sci. USA* **90,** 5345–5349.
22. Keck, M. V. & Lippard, S. J. (1992) *J. Am. Chem. Soc.* **114,** 3386–3390.
23. Siemens Industrial Automation (1996) SADABS: *Area-Detector Absorption Correction* (Siemens Industrial Automation, Madison, WI).
24. Sheldrick, G. M. (2001) SHELXTL (Univ. of Göttingen, Göttingen, Germany).
25. Watkin, D. J., Prout, C. K., Carruthers, J. R., Betteridge, P. W. & Cooper, R. I. (2003) CRYSTALS (Chemical Crystallography Laboratory, Oxford, U.K.).
26. Hwang, T.-L. & Shaka, A. J. (1995) *J. Magn. Reson. Ser. A* **112,** 275–279.
27. Farrell, N., Qu, Y., Bierbach, U., Valsecchi, M. & Menta, E. (1999) in *Cisplatin: Chemistry and Biochemistry of a Leading Anticancer Drug*, ed. Lippert, B. (Wiley, Weinheim, Germany), pp. 479–496.
28. Stanley, K. & Baird, M. C. (1975) *J. Am. Chem. Soc. I* **97,** 6598–6599.
29. Pasternack, R. F., Gibbs, E. J. & Villafranca, J. J. (1983) *Biochemistry* **22,** 2406–2414.
30. Farrell, N., Appleton, T. G., Qu, Y., Roberts, J. D., Soares Frontes, A. P., Skov, K. A., Wu, P. & Zou, Y. (1995) *Biochemistry* **34,** 15480–15486.
31. Brabec, V., Kašpárková, J., Vrána, O., Nováková, O., Cox, J. W., Qu, Y. & Farrell, N. (1999) *Biochemistry* **38,** 6781–6790.
32. Barton, J. K., Basile, L. A., Danishefsky, A. & Alexandrescu, A. (1984) *Proc. Natl. Acad. Sci. USA* **81,** 1961–1965.
33. Barton, J. K. & Lolis, E. (1985) *J. Am. Chem. Soc.* **107,** 708–709.
34. Grover, N., Gupta, N. & Thorp, H. H. (1992) *J. Am. Chem. Soc.* **114,** 3390–3393.
35. Bostock-Smith, C. E., Harris, S. A., Laughton, C. A. & Searle, M. S. (2001) *Nucleic Acids Res.* **29,** 693–702.
36. Zamble, D. & Lippard, S. J. (1999) in *Cisplatin: Chemistry and Biochemistry of a Leading Anticancer Drug*, ed. Lippert, B. (Wiley, Weinheim, Germany), pp. 73–110.